CommonRoad-CriMe: A Toolbox for Criticality Measures of Autonomous Vehicles

Yuanfei Lin and Matthias Althoff

***Abstract*— Criticality measures are essential for autonomous vehicles to capture the complexity of the surrounding environment, trigger emergency maneuvers, and verify safety. However, there is currently no publicly available toolbox that allows researchers to use or evaluate a large number of criticality measures on arbitrary traffic scenarios. To address this issue, we present `CommonRoad-CriMe`, an open-source toolbox for measuring the criticality of autonomous vehicles in a unified framework. Our toolbox covers a wide range of state-of-the-art criticality measures and provides visualized information to facilitate debugging and showcasing. Numerical experiments demonstrate how our toolbox facilitates the comparison of different criticality measures and the analysis of traffic conflicts. Our toolbox is available at commonroad.in.tum.de.**

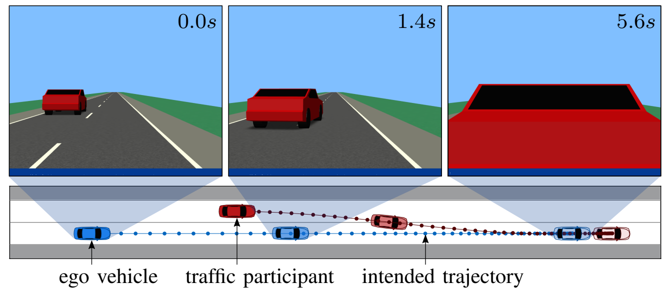

Fig. 1: An exemplary critical scenario in which the other traffic participant (red) cuts into the lane of the ego vehicle (blue) and brakes hard. The snapshots[1] show the inside view of the ego vehicle at three time steps.

I. Introduction

Automotive manufacturers must ensure that autonomous vehicles can recognize and effectively handle unexpected situations. To achieve this, criticality measures (aka *surrogate indicators* or *threat assessments*) are often used to identify safety-critical scenarios and validate autonomous driving systems [1]. A literature review on criticality measures for autonomous driving can be found in [2]–[6]. For the scope of this paper, criticality refers to the level of risk for the involved vehicles with respect to the continuation of a certain traffic situation [1, Def. 1]. An example of a critical scenario is shown in Fig. 1. Despite decades of research, the authors are unaware of any open-source toolbox available for applying and comparing different criticality measures to a wide range of scenarios, as addressed by our work.

A. Related Work

Subsequently, we present related works on criticality measures for advanced driver assistant systems and autonomous driving as well as existing open-source toolboxes computing criticality measures.

a) Criticality Measures for Advanced Driver Assistant Systems and Autonomous Driving: Criticality measures are primarily developed to objectively determine the behavioral safety and threat level of autonomous driving systems. For example, criticality measures are used to validate the safety of autonomous vehicles through various methods, including generating safety-critical scenarios [7]–[11], falsifying the system under test [12], and formally verifying system properties [1]. For motion planning applications, criticality measures help to find traffic conflicts, repair unsafe trajectories, and provide fail-safe solutions [13]–[15].

Model-based and data-driven methods are frequently used to estimate the criticality of a traffic situation [2], [3]. The criticality is influenced, e.g., by the likelihood and consequence of a collision or other dangerous situations. However, due to the large number and variety of existing criticality measures in the literature, selecting the appropriate measure for a particular traffic scenario is challenging.

b) Existing Toolboxes with Criticality Measures: There are several publicly available toolkits that include safety and criticality measures. For example, the Apollo open platform[2] defines a limited number of safety and comfort metrics for grading simulated scenarios. Meanwhile, the open-source simulation platform CARLA [16] embeds the responsible-sensitive safety model [17], which identifies safety-critical situations. Although these tools emulate real-world driving environments, they only cover a few criticality measures, and the overhead required to set up the entire simulation environment in C++ makes it difficult to include new measures. Therefore, tools written in easy-to-use programming languages that cover a wide range of criticality measures are desired.

B. Contributions

To effortlessly measure and compare the criticality of an autonomous vehicle, referred to as *ego vehicle* in the following sections, we present the novel CommonRoad Criticality Measures (`CommonRoad-CriMe`) toolbox, which:

1) provides a framework in Python with unified notations, vehicle models, and coordinate systems for criticality measures;
2) adopts and supplements the categorization of criticality measures defined in [6];

The authors are with the School of Computation, Information and Technology, Technical University of Munich, 85748 Garching, Germany.
`{yuanfei.lin, althoff}@tum.de`

[1]The snapshots are created with esmini, see `https://github.com/esmini/esmini`.

[2]`https://github.com/ApolloAuto/apollo`

3) is open-source and allows users to easily modify, add, and compare criticality measures; and
4) offers efficient and reliable computation by bridging to powerful scenario evaluation tools, such as a drivability checker [18], a scenario designer [19], a set-based predictor [20], and a reachability analyzer [21].

The remainder of this work is structured as follows: Sec. II introduces required preliminaries and definitions. Sec. III provides an overview and a list of representative measures in the toolbox. In Sec. IV, we showcase the benefits of `CommonRoad-CriMe` with numerical examples. Finally, Sec. V concludes the paper.

II. Preliminaries

A. System Description

We model the motion of vehicles as discrete-time systems:

$$\boldsymbol{x}_{k+1} = f_d(\boldsymbol{x}_k, \boldsymbol{u}_k), \tag{1}$$

where $\boldsymbol{x}_k \in \mathbb{R}^{n_x}$ is the state vector, $\boldsymbol{u}_k \in \mathbb{R}^{n_u}$ is the input vector, and the index $k \in \mathbb{N}_0$ maps to a discrete time step according to $t_k = k\Delta t$ with Δt being a fixed time increment. At each time step, the system is bounded by sets of admissible states $\mathcal{X}_k \subset \mathbb{R}^{n_x}$ and admissible control inputs $\mathcal{U}_k \subset \mathbb{R}^{n_u}$. We use the notation $\chi(k', \boldsymbol{x}_k, \boldsymbol{u}_{[k,k']})$ to represent the solution of (1) at time step $k' \geq k$, given an initial state $\boldsymbol{x}_k$ and an input trajectory $\boldsymbol{u}_{[k,k']}$ for the time interval $[k, k']$. Due to limited space, we use the shorthand $\chi_{k'} := \chi(k', \boldsymbol{x}_k, \boldsymbol{u}_{[k,k']})$.

The state vector of a vehicle $\boldsymbol{x}^{\mathtt{G}} := (s_x, s_y, v, \theta)^T$ in a global Cartesian coordinate frame G typically consists at least of the position $(s_x, s_y)^T$, the velocity v, and the heading θ as the basic elements. Other models have either state variables that can be converted to the previous ones and/or further state variables that are irrelevant to this work. Considering the criticality measures based on structured road scenarios, we can localize the vehicle in curvilinear coordinate systems L [22] formulated locally with respect to a reference path Γ, e.g., the centerline of the road. As shown in Fig. 2, the vehicle is described by the longitudinal position s_ξ, the orthogonal deviation of the reference path s_η, and the relative heading $e_\theta := \theta - \theta_\Gamma(s_\xi)$ measured with respect to Γ with orientation $\theta_\Gamma(s_\xi)$. When localizing a point-mass vehicle model in the curvlinear coordinate system, the state vector is denoted as $\boldsymbol{x}^{\mathtt{L}} := (s_\xi, s_\eta, v_\xi, v_\eta)^T$ and the system receives inputs $\boldsymbol{u}^{\mathtt{L}} := (a_\xi, a_\eta)^T$. For brevity, we omit the superscript when it is clear which coordinate system is being used based on the context.

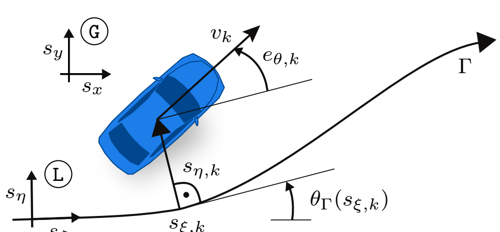

Fig. 2: Vehicle localization in the global Cartesian frame G and the curvilinear coordinate system L aligned with a reference path Γ.

Let $\square$ be a variable, we denote its value associated with the ego vehicle by $\square_{\text{ego}}$ and with the obstacle $b \in \mathcal{B}$ by $\square_b$, where $\mathcal{B}$ is the set of all criticality-relevant obstacles. The functions $\text{front}(\boldsymbol{x}_k) : \mathbb{R}^{n_x} \to \mathbb{R}$, $\text{rear}(\boldsymbol{x}_k) : \mathbb{R}^{n_x} \to \mathbb{R}$, $\text{occ}(\boldsymbol{x}_k) : \mathbb{R}^{n_x} \to \mathrm{P}(\mathbb{R}^2)$[3], and $\text{lanes}(\boldsymbol{x}_k) : \mathbb{R}^{n_x} \to \mathrm{P}(\mathbb{N}_0)$ return the position of the front bumper, rear bumper, the spatial occupancy, and the indices of occupied lanes of a vehicle at time step k, respectively. Given the occupancy of an obstacle b at time step k, we denote the set of forbidden state for the ego vehicle as $\mathcal{F}(\boldsymbol{x}_{b,k}) := \{\boldsymbol{x}_{\text{ego},k} \in \mathcal{X}_k \mid \text{occ}(\boldsymbol{x}_{\text{ego},k}) \cap \text{occ}(\boldsymbol{x}_{b,k}) \neq \emptyset\}$.

B. Definitions

The following definitions are necessary for introducing the presented criticality measures:

Definition 1 (Maneuver $\mathtt{m}$): *A maneuver $\mathtt{m}$ is an element of the set that consists of braking, constant velocity, kickdown, steering, turning, overtaking, and lane change.*

The control input of a vehicle with maneuver $\mathtt{m}$ is denoted as $\boldsymbol{u}^{\mathtt{m}}$. In other works, e.g., [23]–[25], the terms action and behavior are used interchangeably for the same purposes as maneuver.

Definition 2 (Scene and Scenario [26, Sec. II and VI]): *A scene is a snapshot of the environment, which includes the lane network as well as states and inputs of vehicles. A scenario is a temporal sequence of maneuvers and scenes.*

Definition 3 (Criticality Measure c [1, Def. 12]): *A criticality measure $c : \mathcal{X}_k^{|\mathcal{B}|+1} \times (\bigtimes_{\tau=k}^{k+h} \mathcal{U}_\tau)^{|\mathcal{B}|+1} \to \mathbb{R}$ is a function that maps the vehicle states and/or inputs to the criticality of a traffic scene at time step k, where $h \in \mathbb{N}_0$ is the prediction horizon of the input trajectory $\boldsymbol{u}_{[k,k+h]}$.*

Monotonicity is a desired relationship between the criticality measure and criticality [27, Def. 1]. For instance, criticality increases as the time-to-collision (TTC) decreases [28]. If the measure input only contains information about the ego vehicle, criticality is computed as the minimum or maximum value[4] of all pairs of the ego and other vehicles, depending on its monotonic relationship to the measure:

$$\begin{aligned} &c(\boldsymbol{x}_{\text{ego},k}, \boldsymbol{u}_{\text{ego},[k,k+h]}) \\ &= \min_{b\in\mathcal{B}} / \max_{b\in\mathcal{B}} c(\boldsymbol{x}_{\text{ego},k}, \boldsymbol{x}_{b,k}, \boldsymbol{u}_{\text{ego},[k,k+h]}, \boldsymbol{u}_{b,[k,k+h]}). \end{aligned} \tag{2}$$

Definition 4 (Reachable Set $\mathcal{R}$ [29, (1)]): *The reachable set at time step k' is the set of states that can be reached from the initial set of states $\mathcal{X}_k$ including measurement uncertainties while avoiding any forbidden states from time step k to k':*

$$\begin{aligned} \mathcal{R}_{k'}(\mathcal{X}_k, \boldsymbol{x}_{b,k}, \boldsymbol{u}_{b,[k,k']}) := \Big\{ \chi_{k'} \Big| &\exists \boldsymbol{x}_k \in \mathcal{X}_k, \forall \tau \in [k, k'], \\ &\exists \boldsymbol{u}_\tau \in \mathcal{U}_\tau : \chi(\tau, \boldsymbol{x}_k, \boldsymbol{u}_{[k,\tau]}) \notin \mathcal{F}\big(\chi_b(\tau, \boldsymbol{x}_{b,k}, \boldsymbol{u}_{b,[k,\tau]})\big) \Big\}. \end{aligned}$$

[3] $\mathrm{P}(\diamond)$ is the power set of $\diamond$.

[4] Maximum is for positive monotonic relationships, whereas minimum is for negative ones. For measures that operate on sets, the infimum or supremum is used.

TABLE I: List of state-of-the-art criticality measures[5]. We express the positive and negative monotonic relationship between the measure and the criticality as $\oplus$ and $\ominus$, respectively.

Domain	Measure	Acronym	Output Range	Mono.	Unit	Implemented Coord. Sys.	Source
Time	Time headway	THW	$\mathbb{R}_+ \cup \{\infty\}$	$\ominus$	s	L	[30]
	Encroachment time	ET	$\mathbb{R}_+ \cup \{\infty\}$	$\ominus$	s	L	[31]
	Post-encroachment time	PET	$\mathbb{R}_+ \cup \{\infty\}$	$\ominus$	s	L	[31]
	Accepted gap size	AGS	$\mathbb{R}_+$	$\ominus$	s	L	[32]
	Time-to-collision	TTC	$\mathbb{R}_+ \cup \{\infty\}$	$\ominus$	s	L	[28]
	Time-to-collision with given prediction	TTC*	$\mathbb{R}_+ \cup \{\infty\}$	$\ominus$	s	G	[33]
	Potential time-to-collision	PTTC	$\mathbb{R}_+ \cup \{\infty\}$	$\ominus$	s	L	[34]
	Worst-time-to-collision	WTTC	$\mathbb{R}_+ \cup \{\infty\}$	$\ominus$	s	G	[35]
	Time-exposed time-to-collision	TET	$\mathbb{R}_+$	$\oplus$	s	L	[23]
	Time-integrated time-to-collision	TIT	$\mathbb{R}_+$	$\oplus$	s^2	L	[23]
	Time-to-closest-encounter	TTCE	$\mathbb{R}_+ \cup \{\infty\}$	$\ominus$	s	L	[36]
	Time-to-zebra	TTZ	$\mathbb{R}_+ \cup \{\infty\}$	$\ominus$	s	L	[37]
	Time-to-brake	TTB	$\mathbb{R}_+ \cup \{\infty, -\infty\}$	$\ominus$	s	L, G	[38], [39]
	Time-to-kickdown	TTK	$\mathbb{R}_+ \cup \{\infty, -\infty\}$	$\ominus$	s	L, G	[38], [39]
	Time-to-steer	TTS	$\mathbb{R}_+ \cup \{\infty, -\infty\}$	$\ominus$	s	L, G	[38], [39]
	Time-to-maneuver	TTM	$\mathbb{R}_+ \cup \{\infty, -\infty\}$	$\ominus$	s	L, G	[38], [39]
	Time-to-react	TTR	$\mathbb{R}_+ \cup \{\infty, -\infty\}$	$\ominus$	s	L, G	[38], [39]
	Worst-time-to-react	WTTR	$\mathbb{R}_+ \cup \{\infty, -\infty\}$	$\ominus$	s	L, G	[33]
	Time-to-violation	TV	$\mathbb{R}_+ \cup \{\infty\}$	$\ominus$	s	L, G	[14]
	Time-to-comply	TC	$\mathbb{R}_+ \cup \{\infty, -\infty\}$	$\ominus$	s	L, G	[14]
Distance	Headway	HW	$\mathbb{R}_+ \cup \{\infty\}$	$\ominus$	m	L	[30]
	Distance-of-closest-encounter	DCE	$\mathbb{R}_+ \cup \{\infty\}$	$\ominus$	m	L	[36]
	Acceptable minimum stopping distance	MSD	$\mathbb{R}_+$	$\oplus$	m	L	[31]
	Proportion of stopping distance	PSD	$\mathbb{R}_+$	$\ominus$	–	L	[31]
Velocity	Delta-v	Delta-v	$\mathbb{R}$	$\oplus$	m/s	L, G	[40], [41]
	Conflict severity	CS	$\mathbb{R}$	$\oplus$	m/s	L, G	[41]
Acceleration	Deceleration-to-safety-time	DST	$\mathbb{R}$	$\oplus$	m/s^2	L	[42]
	Required longitudinal acceleration (aka deceleration rate to avoid crash)	$a_{\xi,\mathrm{req}}$ (DRAC)	$\mathbb{R}_-$	$\ominus$	m/s^2	L	[30], [43]
	Required lateral acceleration	$a_{\eta,\mathrm{req}}$	$\mathbb{R}_+$	$\oplus$	m/s^2	L	[30]
	Required acceleration	a_{req}	$\mathbb{R}_+$	$\oplus$	m/s^2	L	[30]
Jerk[6]	Longitudinal jerk	LongJ	$\mathbb{R}_+$	$\oplus$	m/s^3	L	[41]
	Lateral jerk	LatJ	$\mathbb{R}_+$	$\oplus$	m/s^3	L	[44], [45]
Index	Conflict index	CI	$[0, 1]$	$\oplus$	$kg{\cdot}m^2/s^2$	L	[46]
	Crash potential index	CPI	$[0, 1]$	$\oplus$	–	L	[43]
	Aggregated crash index	ACI	$\mathbb{R}_+$	$\oplus$	–	L	[47]
	Trajectory criticality index	TCI	$\mathbb{R}_+$	$\oplus$	–	G	[48]
	Pedestrian risk index	PRI	$\mathbb{R}_+$	$\oplus$	m^2/s^3	L	[49]
	Space occupancy index	SOI	$\mathbb{R}_+$	$\oplus$	$1/m^2$	L, G	[50]
	Brake threat number	BTN	$\mathbb{R}_+$	$\oplus$	–	L	[30], [51]
	Steer threat number	STN	$\mathbb{R}_+$	$\oplus$	–	L	[30], [51]
	Responsibility sensitive safety-dangerous situation	RSS	$\{0, 1\}$	$\oplus$	–	L	[17]
Reachable-Set	Drivable area	DA	$\mathbb{R}_+$	$\ominus$	m^2	L, G	[7]–[9]
Probability	Collision probability via Monte Carlo simulation	P-MC	$[0, 1]$	$\oplus$	–	L, G	[24], [52]
	Collision probability via scoring multiple hypotheses	P-SMH	$[0, 1]$	$\oplus$	–	L, G	[53]
	Collision probability via stochastic reachable sets	P-SRS	$[0, 1]$	$\oplus$	–	L, G	[54]
Potential	Potential functions as superposition of scoring functions	PF	$\mathbb{R}$	$\oplus$	–	L, G	[55]
	Safety potential	SP	$\mathbb{R}_+$	$\oplus$	–	L, G	[56]

[5]The categorization is based on [6], of which the up-to-date descriptions can be found at `https://criticality-metrics.readthedocs.io`.

[6]We take the absolute jerk since the sign is insignificant for the criticality and affects the monotonic relationship.

III. COMMONROAD-CRIME

A. Overview

The architecture of `CommonRoad-CriMe` is depicted in Fig. 3 as a unified modeling language (UML) class diagram.

We provide the user interface for setting configurations, selecting criticality measures, and loading traffic scenarios in the class `CriMeInterface`. The class `Scenario` [57] contains the information of a series of continuous traffic scenes (class `Scene`). The criticality measures are defined in the core module `Measure`, of which the categorization is based on their output domains adapted from [6] (cf. Tab. I). It should be noted that there are numerous criticality measures in the literature and new ones are continually being developed, making it impossible to cover them all. However, in the following sections, we provide a representative list of them and aim to use the most prominent definitions for a comprehensive analysis. Please note that our calculation does not take into account discretization errors or vehicle reaction time. We reset time for each evaluation without loss of generality.

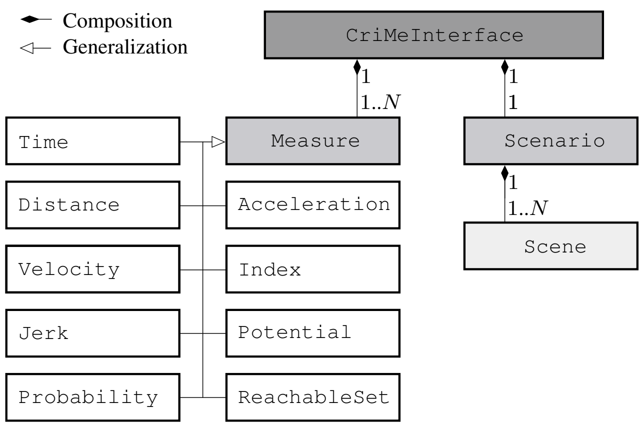

Fig. 3: UML class diagram of `CommonRoad-CriMe`.

B. Headway and Time Headway

The headway (HW) is the distance from the ego vehicle to the leading vehicle. Since the distance along the lane centerline is more representative than the straight-line distance [58], the HW is defined in the curvilinear coordinate system [30, Sec. 5.3.1]:

$$
\begin{aligned}
&HW(\boldsymbol{x}_{\text{ego},k}, \boldsymbol{x}_{b,k})\\
&= \begin{cases}
\text{rear}(\boldsymbol{x}^{\mathtt{L}}_{b,k}) - \text{front}(\boldsymbol{x}^{\mathtt{L}}_{\text{ego},k}) & \text{if lanes}(\boldsymbol{x}_{\text{ego},k}) \cap \text{lanes}(\boldsymbol{x}_{b,k}) \neq \emptyset \\
& \quad \text{and rear}(\boldsymbol{x}^{\mathtt{L}}_{b,k}) \geq \text{front}(\boldsymbol{x}^{\mathtt{L}}_{\text{ego},k}), \\
\infty & \text{otherwise.}
\end{cases}
\end{aligned}
$$

Similarly, the time headway (THW) is the time until the ego vehicle reaches the position of the leading vehicle [30, Sec. 5.3.1]. Assuming the ego vehicle drives at a constant velocity, the THW is [30, (5.23)]:

$$
THW(\boldsymbol{x}_{\text{ego},k}, \boldsymbol{x}_{b,k}) = \frac{HW(\boldsymbol{x}_{\text{ego},k}, \boldsymbol{x}_{b,k})}{v_{\xi,\text{ego},k}}.
$$

C. Time-To-X

The most used criticality measure is time-to-x (TTX), where x denotes a relevant event on the path toward a potential collision.

1) Time-To-Collision: TTC is a measure of the time remaining until a collision occurs [2]. When calculating the TTC, we often assumed that the relative acceleration between vehicles is zero [23] or constant [30, Sec. 5.3.2]. Without loss of generality, we consider the latter case and compute the TTC based on the HW, the relative velocity $\Delta v_\xi := v_{\xi,b} - v_{\xi,\text{ego}}$, and the relative acceleration $\Delta a_\xi := a_{\xi,b} - a_{\xi,\text{ego}}$ in ξ-direction [30, (5.26)]:

$$
\begin{aligned}
&TTC(\boldsymbol{x}_{\text{ego},k}, \boldsymbol{x}_{b,k})\\
&= \begin{cases}
-\frac{HW(\dots)}{\Delta v_{\xi,k}} & \text{if } \Delta v_{\xi,k} < 0 \text{ and } \Delta a_\xi = 0, \\
\infty & \text{if } \Delta v_{\xi,k}^2 - 2HW(\dots)\Delta a_{\xi,k} < 0, \\
-\frac{\Delta v_{\xi,k}}{\Delta a_{\xi,k}} - \frac{\sqrt{\Delta v_{\xi,k}^2 - 2HW(\dots)\Delta a_{\xi,k}}}{\Delta a_{\xi,k}} & \text{if } \Delta v_{\xi,k} < 0 \text{ and } \Delta a_{\xi,k} \neq 0, \\
-\frac{\Delta v_{\xi,k}}{\Delta a_{\xi,k}} - \frac{\sqrt{\Delta v_{\xi,k}^2 - 2HW(\dots)\Delta a_{\xi,k}}}{\Delta a_{\xi,k}} & \text{if } \Delta v_{\xi,k} \geq 0 \text{ and } \Delta a_{\xi,k} < 0, \\
\infty & \text{otherwise.}
\end{cases}
\end{aligned}
$$

A more accurate alternative is to compute the TTC with an intended trajectory of the ego vehicle and the given prediction of other vehicles [13], [33], which we call TTC*. Given a most-likely or set-based prediction [59] of a vehicle b, we define that the intended trajectory of the ego vehicle can be executed without collisions through the predicate

$$
\begin{aligned}
&\texttt{noCollision}(\boldsymbol{x}_{\text{ego},k}, \boldsymbol{x}_{b,k}, \boldsymbol{u}_{\text{ego},[k,k+h]}, \boldsymbol{u}_{b,[k,k+h]}) \iff \\
&\qquad \forall k' \in [k, k+h]: \ \chi_{\text{ego},k'} \notin \mathcal{F}(\chi_{b,k'}).
\end{aligned}
$$

TTC* is then computed by [33, Def. 1]:

$$
\begin{aligned}
&TTC^*(\boldsymbol{x}_{\text{ego},k}, \boldsymbol{x}_{b,k}, \boldsymbol{u}_{\text{ego},[k,k+h]}, \boldsymbol{u}_{b,[k,k+h]})\\
&= \begin{cases}
\infty & \text{if } \texttt{noCollision}(\dots) \text{ holds,} \\
\min \left\{ t_{k'-k} \middle| k' \in [k, k+h], \chi_{\text{ego},k'} \in \mathcal{F}(\chi_{b,k'}) \right\} & \text{otherwise.}
\end{cases}
\end{aligned}
$$

2) Time-To-Collision Variants: Based on the TTC, the time-exposed time-to-collision (TET) and time-integrated time-to-collision assess the criticality considering future vehicle trajectories over space and time [23]. Since the effectiveness of TTC decreases significantly in the lateral direction of the ego vehicle, the encroachment time (ET) and post-encroachment time (PET) are proposed to measure traffic conflicts in intersections [31]. A similar approach is employed for the time-to-closest-encounter (TTCE) and distance-to-closest-encounter (DCE), which generalizes the TTC to non-collision cases [36]. To obtain a worst-case approximation, the TTC is extended to the worst-time-to-collision (WTTC) in [35], which takes lateral traffic into account and tends to overestimate the criticality of traffic scenarios.

3) Time-To-Maneuver and Time-To-React: The TTC and its variants do not provide enough information for collision avoidance, as they do not include possible evasive maneuvers [33]. To address this limitation, the time-to-maneuver (TTM) is proposed as the latest possible time before the TTC*, at which an evasive maneuver still exists [39, (8)]:

$$
\begin{aligned}
&TTM(\boldsymbol{x}_{\text{ego},k}, \boldsymbol{x}_{b,k}, \boldsymbol{u}_{\text{ego},[k,k+h]}, \boldsymbol{u}_{b,[k,k+h]})\\
&= \begin{cases}
\infty & \text{if } \texttt{noCollision}(\dots) \text{ holds,} \\
\max\Bigg(\Big\{-\infty\Big\} \cup \Big\{ t_{k'-k} \Big| k' \in [k, k+TTC^*(\dots)], \exists \boldsymbol{u}^{\mathtt{m}}_{\text{ego},[k',k+h]} \subset \mathcal{U}: \\
\texttt{noCollision}(\dots, [\boldsymbol{u}_{\text{ego},[k,k')}, \boldsymbol{u}^{\mathtt{m}}_{\text{ego},[k',k+h]}], \dots) \Big\}\Bigg) & \text{otherwise.}
\end{cases}
\end{aligned}
$$

For emergency braking, evasive steering, and kickdown, the corresponding TTM is denoted as the time-to-brake (TTB), time-to-steer (TTS), and time-to-kickdown (TTK), respectively. In [38], the authors propose the time-to-react (TTR) as the maximum TTM of all possible maneuvers. Since computing the exact TTR is computationally intractable [33], the TTR is underapproximated using a set of selected evasive maneuvers [39, (10)]:

$$TTR(\boldsymbol{x}_{\text{ego},k}, \boldsymbol{x}_{b,k}, \boldsymbol{u}_{\text{ego},[k,k+h]}, \boldsymbol{u}_{b,[k,k+h]}) = \max\big(TTB(\dots), TTS(\dots), TTK(\dots)\big).$$

In contrast, the TTR is tightly overapproximated by iteratively checking the existence of collision-free reachable sets of the ego vehicle, which is denoted as the worst-time-to-react (WTTR) [33, Prop. 1]:

$$WTTR(\boldsymbol{x}_{\text{ego},k}, \boldsymbol{x}_{b,k}, \boldsymbol{u}_{\text{ego},[k,k+h]}, \boldsymbol{u}_{b,[k,k+h]}) = \begin{cases} \infty & \text{if } \texttt{noCollision}(\dots) \text{ holds}, \\ \max\Big(\Big\{-\infty\Big\} \cup \Big\{t_{k'-k} \Big| k' \in [k, k+TTC^{*}(\dots)], \\ \mathcal{R}_{k+h}(\chi_{\text{ego},k'}, \chi_{b,k'}, \boldsymbol{u}_{b,[k',k+h]}) \neq \emptyset\Big\}\Big) & \text{otherwise}. \end{cases}$$

D. Delta-v

Delta-v measures the change in velocity a vehicle experiences as a result of a collision, which is widely used for measuring crash severity [40]. Assuming an inelastic collision between vehicles, we compute Delta-v taking their masses M into account [41, (2)]:

$$\textit{Delta-v}(\boldsymbol{x}_{\text{ego},k}, \boldsymbol{x}_{b,k}) = \frac{M_b(v_{\text{ego},k} + v_{b,k}\cos(\theta_{\text{ego},k} - \theta_{b,k}))}{M_{\text{ego}} + M_b}.$$

E. Brake and Steer Threat Number

To measure the difficulty of avoiding a collision with evasive maneuvers, the brake threat number (BTN) and the steer threat number (STN) are proposed in [30, Sec. 8.4.1]. These numbers represent the ratio of the required longitudinal and lateral acceleration $a_{\xi,\text{req},k}$ and $a_{\eta,\text{req},k}$ for collision avoidance at time step k to the maximum available accelerations $a_{\xi,\max}$ and $a_{\eta,\max}$, respectively [30, (5.36), (5.48), and (8.3)]:

$$BTN(\boldsymbol{x}_{\text{ego},k}, \boldsymbol{x}_{b,k}) = -\frac{a_{\xi,\text{req},k}}{a_{\xi,\max}} = \frac{\min(a_{\xi,b,k} - \frac{\Delta v_{\xi,k}^2}{2HW(\dots)}, 0)}{-a_{\xi,\max}},$$

$$STN(\boldsymbol{x}_{\text{ego},k}, \boldsymbol{x}_{b,k}) = \frac{a_{\eta,\text{req},k}}{a_{\eta,\max}} = \frac{1}{a_{\eta,\max}} \min\left(\left|a_{\eta,b,k} - \frac{2\big(-HW(\dots) \pm \frac{w_{\text{ego}}+w_b}{2} - \Delta v_{\eta,k} TTC(\dots)\big)}{TTC^2(\dots)}\right|\right),$$

where w is the width of the vehicle and Δv_η is the relative velocity along the η-axis.

F. Drivable Area

The drivable area is the configuration space in which the ego vehicle can operate safely without colliding [8]. By projecting the reachable set (cf. Def. 4) to the position domain in the Euclidean space, the drivable area at time step k' is obtained by [60, Def. 4]:

$$\mathcal{D}_{k'}(\boldsymbol{x}_{\text{ego},k}, \boldsymbol{x}_{b,k}, \boldsymbol{u}_{b,[k,k+h]}) = \text{proj}_{(s_x,s_y)}\big(\mathcal{R}_{k'}(\boldsymbol{x}_{\text{ego},k}, \boldsymbol{x}_{b,k}, \boldsymbol{u}_{b,[k,k']})\big),$$

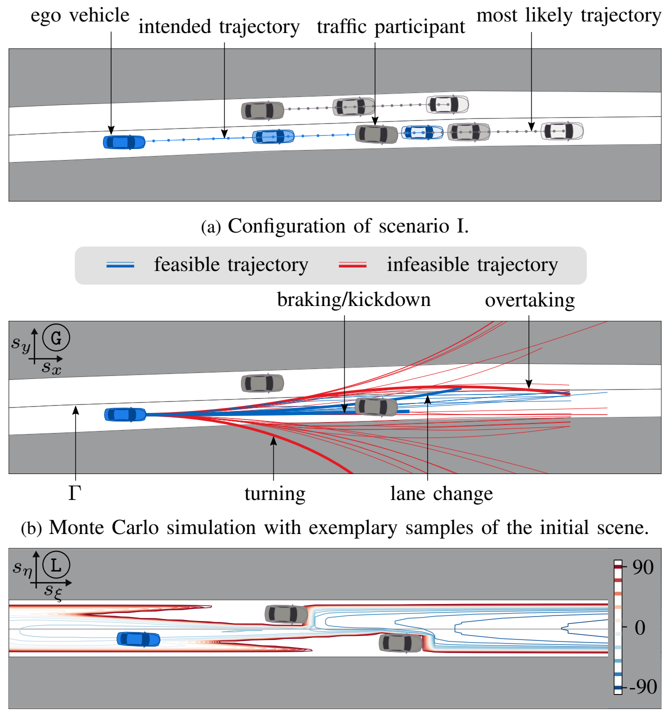

(a) Configuration of scenario I.

(b) Monte Carlo simulation with exemplary samples of the initial scene.

(c) Isopotential contours of the initial scene.

Fig. 4: Configuration and exemplary evaluation results of scenario I[7].

where the operator $\text{proj}_\diamond(\cdot)$ maps a set of states to its elements $\diamond$. The authors in [8] define the area profile of the drivable area over time as a measure of criticality.

G. Collision Probability via Monte Carlo Simulation

The criticality of traffic scenarios can be measured as the probability of a collision [24, (8)]:

$$P(\mathcal{C}) = \int_{U \in (\times_{k'=k}^{k+h} \mathcal{U}_{k'})} P(\mathcal{C}|U)P(U)\mathrm{d}U,$$

where $\mathcal{C}$ is the event of a collision and the control inputs $U := (\boldsymbol{u}_k, \dots, \boldsymbol{u}_{k+h})$ are modeled as random variables. To estimate $P(\mathcal{C})$, Monte Carlo simulation is often used to explore possible realizations of predefined maneuvers by randomly sampling the input space [24], [52], [61]. The collision probability with Monte Carlo simulation is referred to as P-MC. We adopt the importance sampling method defined in [24] and consider the following maneuvers: braking/kickdown, lane change, overtaking, and turning (see Fig. 4b).

H. Potential Functions as Superposition of Scoring Functions

The artificial potential field method uses potential functions (PF) to model the interactions between vehicles and their environment. The PF defined in [55] includes various scoring functions, such as the measure for lane keeping and centering, road geometry, collision avoidance, and target velocity, which are frequently used for non-crash-based criticality assessment. In our toolbox, we extended the approach presented in [55] to handle both straight and curved roads using the curvilinear coordinate system, as shown in Fig. 4c.

[7]CommonRoad ID: DEU_Gar-1_1_T-1

IV. Numerical Examples

We evaluate the criticality of scenes and scenarios from the CommonRoad benchmark suite [57] using `CommonRoad-CriMe` with exemplary measures and show the benefits of using our toolbox. Scenario I, with $h = 20$ and $\Delta t = 0.1s$, depicts a rural environment in which the intended trajectory of the ego vehicle and the most likely trajectories of the other traffic participants are given (cf. Fig. 4a). In the urban scenario II[8], we present a set-based prediction of the other vehicles for $h = 30$ time steps using $\Delta t = 0.25s$ as shown in Fig. 5a. We refer to scenes I and II as the initial scenes of scenarios I and II, respectively. We employ the CommonRoad vehicle models [57] and use the point-mass model to demonstrate the results. The parameters for computing the measures are obtained from the original papers (cf. Tab. I).

A. Evaluation on Scenes

The evaluation results of scenes I and II with selected criticality measures are listed in Tab. II. The TTC is computed as $3.70s$ for scene I (see Fig. 4a) indicating a low criticality. It does, however, rule out the possibility that the leading vehicle fully brakes, implying a high risk for the ego vehicle. This false-negative indication is the same for scene II (see Fig. 5a) when the other participant drifts to the lane of the ego vehicle. Therefore, the TTC is less effective in assessing collision risks in the lateral driving direction. In contrast to TTC, the TTC* allows one to consider a more sophisticated prediction of vehicles, especially the set-based prediction. In Fig. 5a, we can observe a possible collision at TTC* if all the possible behaviors of the other traffic participant are considered. WTTC also attempts to address the inefficiency of using TTC, as shown in Fig. 5b. However, its threshold value for triggering warnings is difficult to define since worst-case scenarios are infrequent in real traffic.

In contrast to the TTC and its variants, TTM and TTR provide evasive trajectories. Fig. 5a shows that the ego vehicle needs to fully brake from the state at TTR, i.e., TTB, to ensure safety. As shown in Fig. 5c, there exist only small drivable areas if the ego vehicle executes evasive maneuvers from the state at time step $^{\mathrm{WTTR}}/_{\Delta t} - 1$.

TABLE II: Criticality measures of scenes I and II.

Measure	Scene I	Scene II	Measure	Scene I	Scene II
HW	22.16	∞	**THW**	1.40	∞
ET	∞	∞	**PET**	∞	∞
TTC	3.70	∞	**WTTC**	0.80	1.10
TTC*	∞	2.25	**TTCE**	1.90	2.25
DCE	1.17	0.00	**TTS**	∞	$-\infty$
TTK	∞	$-\infty$	**TTB**	∞	1.25
TTR	∞	1.25	**WTTR**	∞	2.00
$\boldsymbol{a_{\xi,\mathrm{req}}}$	-0.81	0.00	$\boldsymbol{a_{\eta,\mathrm{req}}}$	0.09	0.00
LongJ	0.00	0.00	**LatJ**	0.00	0.00
BTN	0.0704	0.0000	**STN**	0.0113	0.0000
DA	78.40	647.54	**P-MC**	0.0098	0.0100
Delta-v	14.00	13.92	**PF**	-9.73	-36.70

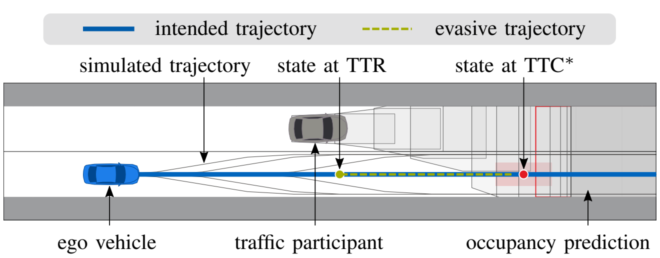

(a) TTC* and TTR. The simulated trajectories are the evasive trajectories for computing the underapproximated TTR.

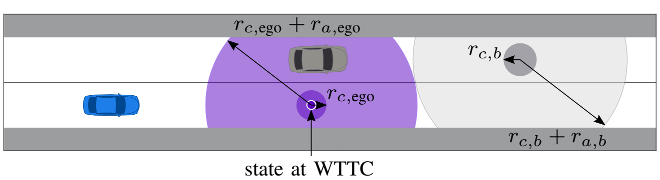

(b) WTTC. The values r_c and r_a denote the radius of the circles approximating the vehicle's shape and of the drivable area for a point-mass vehicle model neglecting the forbidden states, respectively.

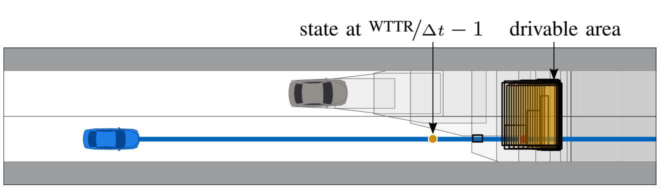

(c) WTTR. The drivable areas are computed starting from time step $^{\mathrm{WTTR}}/_{\Delta t} - 1$ and ending at time step h.

Fig. 5: Evaluation results of scene II.

[8]CommonRoad ID: ZAM_Urban-7_1_S-2

B. Evaluation on Scenarios

Fig. 6 depicts the evaluation results for the entire scenario I. From the profiles of the TTC and $a_{\xi,\mathrm{req}}$, we can see that the ego vehicle is getting closer to the leading vehicle, but the level of criticality with respect to the other traffic participants is unknown. The curves of the BTN, STN, and P-MC indicate that a collision is unlikely to occur in this scenario, as their values are significantly lower than the collision threshold of 1.0 [52], [62]. The DA curve confirms this observation by showing that there are ample collision-free, reachable positions for the ego vehicle in the near future. Instead, the PF reaches its maximum potential starting from time step 10, indicating that the ego vehicle does not maintain a safe distance when the preceding vehicle fully brakes, i.e., safety is not ensured. In conclusion, we can infer that relying on a single criticality measure may not provide enough information, and that multiple measures are required to accurately assess the criticality of a scenario.

We further measure the TTC of 1,000 randomly selected scenarios from the CommonRoad benchmark suite to demonstrate the usefulness of our toolbox. The CommonRoad collection includes a mix of recorded and handcrafted scenarios, such as those on highways, rural roads, and in urban settings. All calculations were carried out on a laptop equipped with an Intel Core i7-1165G7 2.8 GHz processor. There exist 21,713 scenes in total in the selected scenarios, and

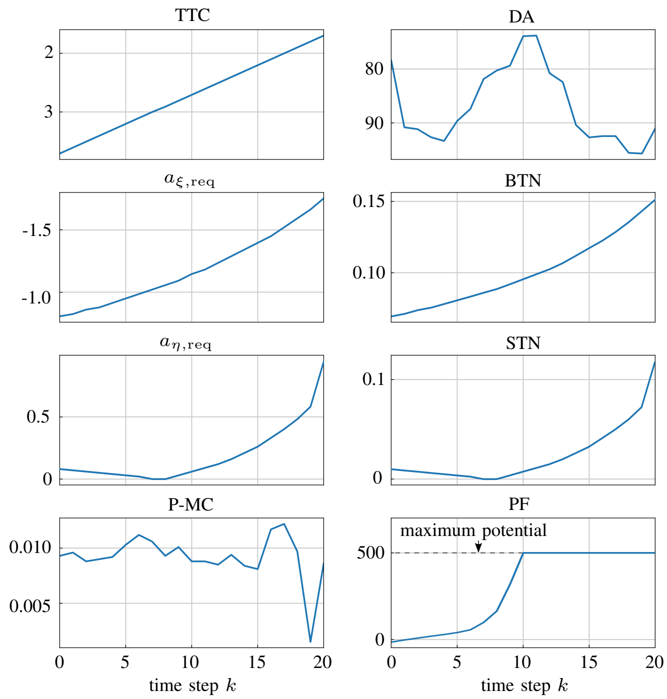

Fig. 6: Criticality profiles of scenario I with exemplary measures. For better insight, the graph's vertical axis indicates an increase in criticality based on the monotonic relationship outlined in Tab. I.

the average computation time of each scene was $17.90ms$ ($1.80ms$ of each vehicle pair). Fig. 7 shows the histogram of the TTC for all scenes in the collection. By analyzing the distribution, we can identify safety-critical situations in the longitudinal driving direction, e.g., using a threshold of TTC $= 1.0s$ [28]. Therefore, `CommonRoad-CriMe` simplifies the process of selecting scenarios of interest from a large database.

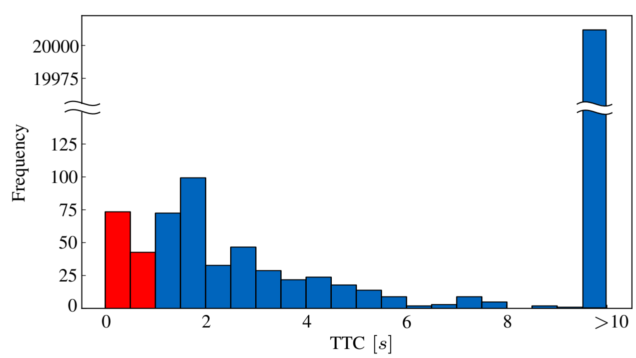

Fig. 7: Histogram of the TTC over 21,713 scenes from the CommonRoad collection. The bins are colored red if the scenes are critical with respect to the TTC and blue otherwise.

V. Conclusions

This paper presents the first toolbox for measuring the criticality of autonomous vehicles that is open-source, easy-to-use, and contains state-of-the-art measures. In `CommonRoad-CriMe`, we provide a unified evaluation framework and support a wide range of criticality measures. We hope that `CommonRoad-CriMe` will make it easier for intelligent transportation researchers to evaluate their autonomous driving functions with various criticality measures and traffic scenarios. Contributions to further improve and expand the capabilities of `CommonRoad-CriMe` are welcomed. Future work includes a more thorough comparison of measures and user studies in order to create a reference for human criticality estimation.

Acknowledgments

We thank Oliver Specht and Ivana Peneva for their contribution to the implementation of some criticality measures. Furthermore, the authors gratefully acknowledge partial financial support by the German Federal Ministry for Digital and Transport (BMDV) within the project *Cooperative Autonomous Driving with Safety Guarantees* (KoSi).

References

[1] C. Neurohr, L. Westhofen, M. Butz, M. H. Bollmann, U. Eberle, and R. Galbas, "Criticality analysis for the verification and validation of automated vehicles," *IEEE Access*, vol. 9, pp. 18 016–18 041, 2021.
[2] S. Lefèvre, D. Vasquez, and C. Laugier, "A survey on motion prediction and risk assessment for intelligent vehicles," *ROBOMECH J.*, vol. 1, no. 1, pp. 1–14, 2014.
[3] J. Dahl, G. R. de Campos, C. Olsson, and J. Fredriksson, "Collision avoidance: A literature review on threat-assessment techniques," *IEEE Trans. on Intell. Veh.*, vol. 4, no. 1, pp. 101–113, 2018.
[4] C. Johnsson, A. Laureshyn, and T. De Ceunynck, "In search of surrogate safety indicators for vulnerable road users: A review of surrogate safety indicators," *Transport Reviews*, vol. 38, no. 6, pp. 765–785, 2018.
[5] S. Riedmaier, T. Ponn, D. Ludwig, B. Schick, and F. Diermeyer, "Survey on scenario-based safety assessment of automated vehicles," *IEEE Access*, vol. 8, pp. 87 456–87 477, 2020.
[6] L. Westhofen, C. Neurohr, T. Koopmann, M. Butz, B. Schütt, F. Utesch, B. Neurohr, C. Gutenkunst, and E. Böde, "Criticality metrics for automated driving: A review and suitability analysis of the state of the art," *Archives of Computational Methods in Engineering*, pp. 1–35, 2022.
[7] M. Klischat and M. Althoff, "Generating critical test scenarios for automated vehicles with evolutionary algorithms," in *Proc. of the IEEE Intell. Veh. Symp.*, 2019, pp. 2352 – 2358.
[8] M. Klischat, E. I. Liu, F. Holtke, and M. Althoff, "Scenario factory: Creating safety-critical traffic scenarios for automated vehicles," in *Proc. of the IEEE Int. Conf. on Intell. Transp. Syst.*, 2020, pp. 1–7.
[9] M. Klischat and M. Althoff, "Synthesizing traffic scenarios from formal specifications for testing automated vehicles," in *Proc. of the IEEE Intell. Veh. Symp.*, 2020, pp. 2065–2072.
[10] X. Zhang, F. Li, and X. Wu, "CSG: Critical scenario generation from real traffic accidents," in *Proc. of the IEEE Intell. Veh. Symp.*, 2020, pp. 1330–1336.
[11] W. Ding, C. Xu, M. Arief, H. Lin, B. Li, and D. Zhao, "A survey on safety-critical driving scenario generation — a methodological perspective," *IEEE Trans. on Intell. Transp. Syst.*, 2023.
[12] M. Klischat and M. Althoff, "Falsifying motion plans of autonomous vehicles with abstractly specified traffic scenarios," *IEEE Trans. on Intell. Veh.*, vol. 8, no. 2, pp. 1717–1730, 2023.
[13] Y. Lin, S. Maierhofer, and M. Althoff, "Sampling-based trajectory repairing for autonomous vehicles," in *Proc. of the IEEE Int. Conf. on Intell. Transp. Syst.*, 2021, pp. 572–579.
[14] Y. Lin and M. Althoff, "Rule-compliant trajectory repairing using satisfiability modulo theories," in *Proc. of the IEEE Intell. Veh. Symp.*, 2022, pp. 449–456.
[15] C. Pek and M. Althoff, "Fail-safe motion planning for online verification of autonomous vehicles using convex optimization," *IEEE Trans. on Robot.*, vol. 37, no. 3, pp. 798–814, 2021.
[16] A. Dosovitskiy, G. Ros, F. Codevilla, A. Lopez, and V. Koltun, "CARLA: An open urban driving simulator," in *Proc. of the Conf. on Robot Learning*, 2017, pp. 1–16.

[17] S. Shalev-Shwartz, S. Shammah, and A. Shashua, "On a formal model of safe and scalable self-driving cars," *arXiv preprint arXiv:1708.06374*, 2018.

[18] C. Pek, V. Rusinov, S. Manzinger, M. C. Üste, and M. Althoff, "CommonRoad Drivability Checker: Simplifying the development and validation of motion planning algorithms," in *Proc. of the IEEE Intell. Veh. Symp.*, 2020, pp. 1013–1020.

[19] S. Maierhofer, M. Klischat, and M. Althoff, "Commonroad Scenario Designer: An open-source toolbox for map conversion and scenario creation for autonomous vehicles," in *Proc. of the IEEE Int. Conf. on Intell. Transp. Syst.*, 2021, pp. 3176–3182.

[20] M. Koschi and M. Althoff, "SPOT: A tool for set-based prediction of traffic participants," in *Proc. of the IEEE Intell. Veh. Symp.*, 2017, pp. 1686–1693.

[21] E. I. Liu, G. Würsching, M. Klischat, and M. Althoff, "CommonRoad-Reach: A toolbox for reachability analysis of automated vehicles," in *Proc. of the IEEE Int. Conf. on Intell. Transp. Syst.*, 2022, pp. 2313–2320.

[22] E. Héry, S. Masi, P. Xu, and P. Bonnifait, "Map-based curvilinear coordinates for autonomous vehicles," in *Proc. of the IEEE Int. Conf. on Intell. Transp. Syst.*, 2017, pp. 1–7.

[23] M. M. Minderhoud and P. H. Bovy, "Extended time-to-collision measures for road traffic safety assessment," *Accident Analysis & Prevention*, vol. 33, no. 1, pp. 89–97, 2001.

[24] A. Broadhurst, S. Baker, and T. Kanade, "Monte Carlo road safety reasoning," in *Proc. of the IEEE Intell. Veh. Symp.*, 2005, pp. 319–324.

[25] Y. Lin, H. Li, and M. Althoff, "Model predictive robustness of signal temporal logic predicates," *arXiv preprint arXiv:2209.07881*, 2022.

[26] S. Ulbrich, T. Menzel, A. Reschka, F. Schuldt, and M. Maurer, "Defining and substantiating the terms scene, situation, and scenario for automated driving," in *Proc. of the IEEE Int. Conf. on Intell. Transp. Syst.*, 2015, pp. 982–988.

[27] A. Majumdar and M. Pavone, "How should a robot assess risk? Towards an axiomatic theory of risk in robotics," *Springer Proc. in Advanced Robot.*, vol. 10, pp. 75–84, 2020.

[28] J. C. Hayward, "Near-miss determination through use of a scale of danger," *Pennsylvania Transp. and Traffic Safety Center, Technical Report*, 1972.

[29] S. Söntges and M. Althoff, "Computing the drivable area of autonomous road vehicles in dynamic road scenes," *IEEE Trans. on Intell. Transp. Syst.*, vol. 19, no. 6, pp. 1855–1866, 2017.

[30] J. Jansson, "Collision Avoidance Theory: With application to automotive collision mitigation," Ph.D. dissertation, Linköping University Electronic Press, 2005.

[31] B. L. Allen, B. T. Shin, and P. J. Cooper, "Analysis of traffic conflicts and collisions," *Transp. Research Record*, vol. 667, pp. 67–74, 1978.

[32] T. Petzoldt, "On the relationship between pedestrian gap acceptance and time to arrival estimates," *Accident Analysis & Prevention*, vol. 72, pp. 127–133, 2014.

[33] S. Soentges, M. Koschi, and M. Althoff, "Worst-case analysis of the time-to-react using reachable sets," in *Proc. of the IEEE Intell. Veh. Symp.*, 2018, pp. 1891–1897.

[34] H. Wakabayashi, Y. Takahashi, S. Niimi, and K. Renge, "Traffic conflict analysis using vehicle tracking system/digital VCR and proposal of a new conflict indicator," *Infrastructure Planning Review*, vol. 20, pp. 949–956, 2003.

[35] W. Wachenfeld, P. Junietz, R. Wenzel, and H. Winner, "The worst-time-to-collision metric for situation identification," in *Proc. of the IEEE Intell. Veh. Symp.*, 2016, pp. 729–734.

[36] J. Eggert, "Predictive risk estimation for intelligent ADAS functions," in *Proc. of the IEEE Int. Conf. on Intell. Transp. Syst.*, 2014, pp. 711–718.

[37] A. Varhelyi, "Drivers' speed behaviour at a zebra crossing: A case study," *Accident Analysis & Prevention*, vol. 30, no. 6, pp. 731–743, 1998.

[38] J. Hillenbrand, A. M. Spieker, and K. Kroschel, "A multilevel collision mitigation approach — its situation assessment, decision making, and performance tradeoffs," *IEEE Trans. on Intell. Transp. Syst.*, vol. 7, no. 4, pp. 528–540, 2006.

[39] A. Tamke, T. Dang, and G. Breuel, "A flexible method for criticality assessment in driver assistance systems," in *Proc. of the IEEE Intell. Veh. Symp.*, 2011, pp. 697–702.

[40] S. G. Shelby *et al.*, "Delta-v as a measure of traffic conflict severity," in *Proc. of the Int. Conf. on Road Safety and Simulation*, 2011, pp. 14–16.

[41] O. Bagdadi, "Estimation of the severity of safety critical events," *Accident Analysis & Prevention*, vol. 50, pp. 167–174, 2013.

[42] C. Hupfer, "Deceleration to safety time (DST) - a useful figure to evaluate traffic safety," in *ICTCT Conf. Proc. of Seminar*, vol. 3, 1997, pp. 5–7.

[43] F. Cunto and F. F. Saccomanno, "Calibration and validation of simulated vehicle safety performance at signalized intersections," *Accident Analysis & Prevention*, vol. 40, no. 3, pp. 1171–1179, 2008.

[44] F. Feng, S. Bao, J. R. Sayer, C. Flannagan, M. Manser, and R. Wunderlich, "Can vehicle longitudinal jerk be used to identify aggressive drivers? An examination using naturalistic driving data," *Accident Analysis & Prevention*, vol. 104, pp. 125–136, 2017.

[45] J. Ambros, J. Altmann, C. Jurewicz, and A. Chevalier, "Proactive assessment of road curve safety using floating car data: An exploratory study," *Archives of Transport*, vol. 50, 2019.

[46] W. K. Alhajyaseen, "The integration of conflict probability and severity for the safety assessment of intersections," *Arabian J. for Science and Engineering*, vol. 40, no. 2, pp. 421–430, 2015.

[47] Y. Kuang, X. Qu, and S. Wang, "A tree-structured crash surrogate measure for freeways," *Accident Analysis & Prevention*, vol. 77, pp. 137–148, 2015.

[48] P. Junietz, F. Bonakdar, B. Klamann, and H. Winner, "Criticality metric for the safety validation of automated driving using model predictive trajectory optimization," in *Proc. of the IEEE Int. Conf. on Intell. Transp. Syst.*, 2018, pp. 60–65.

[49] S. Cafiso, A. G. Garcia, R. Cavarra, and M. R. Rojas, "Crosswalk safety evaluation using a pedestrian risk index as traffic conflict measure," in *Proc. of the Int. Conf. on Road safety and Simulation*, 2011, pp. 1–15.

[50] K. Ogawa, "An analysis of traffic conflict phenomenon of bicycles using space occupancy index," *J. of the Eastern Asia Society for Transp. Studies*, vol. 7, pp. 1820–1827, 2007.

[51] M. Brannstrom, J. Sjoberg, and E. Coelingh, "A situation and threat assessment algorithm for a rear-end collision avoidance system," in *Proc. of the IEEE Intell. Veh. Symp.*, 2008, pp. 102–107.

[52] A. Eidehall and L. Petersson, "Statistical threat assessment for general road scenes using Monte Carlo sampling," *IEEE Trans. on Intell. Transp. Syst.*, vol. 9, no. 1, pp. 137–147, 2008.

[53] E. S. Morales, R. Membarth, A. Gaull, P. Slusallek, T. Dirndorfer, A. Kammenhuber, C. Lauer, and M. Botsch, "Parallel multi-hypothesis algorithm for criticality estimation in traffic and collision avoidance," in *Proc. of the IEEE Intell. Veh. Symp.*, 2019, pp. 2164–2171.

[54] M. Althoff, O. Stursberg, and M. Buss, "Model-based probabilistic collision detection in autonomous driving," *IEEE Trans. on Intell. Transp. Syst.*, vol. 10, no. 2, pp. 299–310, 2009.

[55] M. T. Wolf and J. W. Burdick, "Artificial potential functions for highway driving with collision avoidance," in *Proc. of the IEEE Int. Conf. on Robot. and Autom.*, 2008, pp. 3731–3736.

[56] D. Nistér, H.-L. Lee, J. Ng, and Y. Wang, "The safety force field," *NVIDIA White Paper*, 2019.

[57] M. Althoff, M. Koschi, and S. Manzinger, "CommonRoad: Composable benchmarks for motion planning on roads," in *Proc. of the IEEE Intell. Veh. Symp.*, 2017, pp. 719–726.

[58] C. Katrakazas, M. Quddus, W.-H. Chen, and L. Deka, "Real-time motion planning methods for autonomous on-road driving: State-of-the-art and future research directions," *Transp. Research Part C: Emerging Technologies*, vol. 60, pp. 416–442, 2015.

[59] M. Koschi and M. Althoff, "Set-based prediction of traffic participants considering occlusions and traffic rules," *IEEE Trans. on Intell. Veh.*, vol. 6, no. 2, pp. 249–265, 2020.

[60] S. Manzinger, C. Pek, and M. Althoff, "Using reachable sets for trajectory planning of automated vehicles," *IEEE Trans. on Intell. Veh.*, vol. 6, no. 2, pp. 232–248, 2020.

[61] M. Althoff and A. Mergel, "Comparison of Markov chain abstraction and Monte Carlo simulation for the safety assessment of autonomous cars," *IEEE Trans. on Intell. Transp. Syst.*, vol. 12, no. 4, pp. 1237–1247, 2011.

[62] C. Wang, C. Popp, and H. Winner, "Acceleration-based collision criticality metric for holistic online safety assessment in automated driving," *IEEE Access*, vol. 10, pp. 70 662–70 674, 2022.